Title
Diagnosing the stratosphere-to-troposphere flux of ozone in a chemistry transport model

Journal
Journal of Geophysical Research, 110(D19)

ISSN
0148-0227

Authors
Hsu, Juno
Prather, Micheal J.
Wild, Oliver

Publication Date
2005-10-01

DOI
10.1029/2005JD006045

Diagnosing the stratosphere-to-troposphere flux of ozone in a chemistry transport model

Juno Hsu and Michael J. Prather
Earth System Science, University of California, Irvine, California, USA

Oliver Wild
Frontier Research Center for Global Change, JAMSTEC, Yokohama, Japan

Received 5 April 2005; revised 25 June 2005; accepted 19 July 2005; published 12 October 2005.

[1] Events involving stratosphere-troposphere exchange (STE) of ozone, such as tropopause folds and westerly ducts, are readily identified in observations and models, but a quantitative flux specifying where and when stratospheric ozone is mixed into the troposphere is not readily discerned from either. This work presents a new diagnostic based on determining when stratospheric air is mixed and diluted down to tropospheric abundances (<100 ppb) and hence effectively participates in tropospheric chemistry. The method is applied to two years of high-resolution, global meteorological fields (1.9 degrees, 40 levels) from the ECMWF forecast model derived by U. Oslo for chemistry transport modeling and used in TRACE-P studies. The UCI CTM is run here with linearized stratospheric ozone chemistry (Linoz) and a parameterized tropospheric sink. In terms of events, the CTM accurately follows a March 2001 westerly duct stratospheric intrusion into the tropical eastern Pacific as observed by TOMS and calculates a 48-hour burst of STE O3 flux for that region. The influx associated with the event (0.3 Tg) is much less than the anomalous amount seen as an isolated island in column ozone (1.7 Tg). A climatology of monthly mean STE fluxes is similar for both years (January to December 1997 and May 2000 to April 2001), but the warm phase of ENSO December 1997 is distinctly different from the cold phase of ENSO month December 2000. Global ozone fluxes are about 515 Tg (year 1997) and 550 Tg (year 2000/2001) with an equal amount into each hemisphere, and larger springtime fluxes for both hemispheres. In terms of geographical distribution, Northern Hemisphere regions of high ozone flux follow the jet streams over the oceans in the winter and over the continents in the summer, in agreement with many previous studies. In contrast, we find the largest STE flux is located in the subtropics during late spring, particularly over the Tibetan Plateau in May. This hot spot of STE is not a numerical artifact, it occurs in both meteorological years, and it appears to be caused by the rapid erosion of the tropopause. Ozone fluxes in the Southern
Hemisphere have less variability (either temporal or spatial), and they occur mainly in the subtropical region (25°S–35°S) regardless of season. The poles, throughout the year, show minimal STE O3 flux.

Citation: Hsu, J., M. J. Prather, and O. Wild (2005), Diagnosing the stratosphere-to-troposphere flux of ozone in a chemistry transport model, *J. Geophys. Res.*, *110*, D19305, doi:10.1029/2005JD006045.

1. Introduction

[2] *Brewer* [1949] described the basic overturning of the stratosphere more than fifty years ago, with low-ozone tropospheric air entering the stratosphere in the tropics and high-ozone air returning to the troposphere in the mid and high latitudes; however, calculating stratosphere-troposphere exchange (STE) remains an active and unresolved research topic (see *Holton et al.* [1995], *Plumb* [2002], and *Stohl et al.* [2003a] for reviews). The STE flux of ozone (O_3) is an important component of the tropospheric ozone budget: it is approximately matched by deposition to the surface, it influences the abundance of ozone from the surface to the tropopause, and it is believed to drive some of the observed seasonal variations [see *Logan*, 1999; *Logan et al.*, 1999; *Monks*, 2000]. A quantitative measure of the geographic and temporal distribution of this STE ozone flux is crucial for understanding the budget of tropospheric ozone. For

0148-0227/05/2005JD006045

example, when trying to understand trends or changes in the variability of tropospheric ozone, whether natural or anthropogenic, it is necessary to separate the influence of the stratosphere (e.g., ozone depletion, changes in circulation) from the troposphere (e.g., increasing CH_4 and emissions of NO_x [*Prather and Ehhalt*, 2001]).

[3] The concept of a unique tropopause height that separates the stratosphere above from troposphere below is, in some sense, mythical. Stratospheric air is observed in the troposphere as complex folds and as apparently isolated layers. Thus a single column of air can contain alternating layers of stratospheric and tropospheric air. Moreover, in tropopause folding events, the stratospheric air mass, even though it occurs below tropospheric air, can return to the stratosphere (e.g., the March 2001 westerly duct event described herein). Thus calculation of the STE ozone flux as the net vertical flux crossing a tropopause height is not tenable: on the global and long-term average, it is accurate, but locally it is dominated by noise, i.e., most of the stratospheric air masses moving in and out the tropopause do not mix. Even with the near-complete ''knowledge'' provided in three-dimensional chemistry transport models (CTM), including assimilation models, there is no easy way to calculate the local STE of ozone in terms of fluxes across surfaces. In terms of observations we do not have sufficiently resolved measurements of ozone and meteorological fields to directly derive this quantity either [*World Meteorological Organization*, 1985]. We present here a novel diagnostic approach for a CTM that calculates locally the flux of ozone into the chemical troposphere. Specifically, we want to count the stratospheric ozone molecules as having been transported into the troposphere only when they are irreversibly mixed into and participate in the photochemical regime of the troposphere (e.g., low O_3, high water vapor, high CO and hydrocarbons, fresh NOx).

[4] Several approaches quantifying the STE, mostly of air mass, are available. *Appenzeller and Holton* [1996] derive the net hemispherically integrated, seasonally resolved, extratropical STE by computing the air mass budget of the lowermost stratosphere (the stratospheric middle world). *Schoeberl* [2004] uses the same method but further separates the adiabatic mass flux from the diabatic mass flux crossing the tropopause. However, hemispherically integrated net air mass flux is inadequate for tropospheric ozone chemistry where more detailed spatial and temporal STE distributions are needed. Another commonly used diagnostic method computes the one-way mass flux from the air velocity relative to the tropopause [*Wei*, 1987], but this flux diverges as model resolution increases [*Wirth and Egger*, 1999; *Gettelman and Sobel*, 2000]. In fact, all such flux calculations that include diffusive processes suffer similar divergence if a one-way flux is computed [*Hall and Holzer*, 2003]. Numerous studies [*Danielsen*, 1961; *Chen*, 1995; *Seo and Bowman*, 2002; *Sprenger and Wernli*, 2003] used Lagrangian-based methods to trace the particles crossing the tropopause. *James et al.* [2003] have used a Lagrangian dispersion model with the inclusion of turbulence parameterizations to trace the particles continuously. Recently, *Jing et al.* [2004] applied a contour advection technique to study the isentropic mass transport across the dynamical tropopause. For ozone flux, *Olsen et al.* [2002] and *Jing et al.* [2004] used the empirical relationship between potential vorticity (PV) and O_3 to derive the ozone flux implied by the rate of PV destruction. *Olsen et al.* [2004] compute the extratropical, 5-year mean net ozone flux explicitly by convolving the mass flux and the ozone mixing ratio produced in Goddard CTM. In their study, the diabatic and adiabatic components of the ozone fluxes are calculated separately with the spatial distribution only available from the diabatic component. Ozone fluxes of different origins from the stratosphere or troposphere are also calculated separately.

[5] Despite the numerous studies analyzing the global cross-tropopause mass flux (a vast literature of case studies is not mentioned here), there appears to be no agreement as to when and where stratospheric O_3 enters the troposphere. There is, however, a mounting convergence on the net annual STE flux of O_3 being in the range 400–600 Tg-O_3/year [*Murphy and Fahey*, 1994; *McLinden et al.*, 2000; *Olsen et al.*, 2001]. A few studies show that the cross-tropopause air mass flux has a late spring/early summer maximum in the Northern Hemisphere [*Appenzeller and Holton*, 1996; *Gettelman and Sobel*, 2000; *Seo and Bowman*, 2002; *Schoeberl*, 2004]. *James et al.* [2003], however, argue that deep intrusion events, which are effective in transporting stratospheric air into the lower troposphere, have a clear winter maximum. In general most studies find that the maximum distributions of stratosphere-troposphere exchange are associated with midlatitude baroclinic activities such as cut-off cyclones and tropopause folds within the storm tracks. The relative STE locations within the storm tracks are quite different for the different studies [see *Gettelman and Sobel*, 2000, Figure 5; *Seo and Bowman*, 2002, Figure 3; *Stohl et al.*, 2003b, Figure 3a; *Sprenger and Wernli*, 2003, Figure 2]. On the other hand, studies focusing on isentropic mass flux across the subtropical jet find the summer/fall maximum in the subtropics, associated with summer monsoon and large-scale wave breaking over the Pacific and Atlantic oceans [*Chen*, 1995; *Postel and Hitchman*, 1999; *Jing et al.*, 2004]. Deep tropical intrusions of ozone occur in equatorial westerly ducts (regions of westerly winds in the tropics bounded by the zero-wind lines), preferentially in the winter [*Waugh and Polvani*, 2000; *Waugh and Funatsu*, 2003], but ozone flux associated with individual events has never been quantified. None of the previous global analysis studies show any significant contributions over the regions of deep tropical intrusion.

[6] This study is motivated in part by the ability to model quantitatively the intrusion of stratospheric ozone into the tropical troposphere at a westerly duct as observed by satellite in March 2001. We develop here a new and direct diagnostic of the STE ozone flux from our Chemistry Transport Model, which in these examples is driven by ECMWF pieced forecast meteorology. The performance of this FRSGC/UCI CTM driven by ECMWF forecast meteorology has been extensively validated during the NASA Transport and Chemical Evolution over the Pacific (TRACE-P) measurement campaign [*Wild et al.*, 2003, 2004; *Kiley et al.*, 2003; *Hsu et al.*, 2004]. We diagnose the net STE ozone flux every 1-hour time step and at each model grid point. Since this flux is dominated by the one-way stratosphere-to-troposphere transport, we can compare with the one-way pattern from previous studies. By correlating the location and timing of the ozone flux with the meteorology,

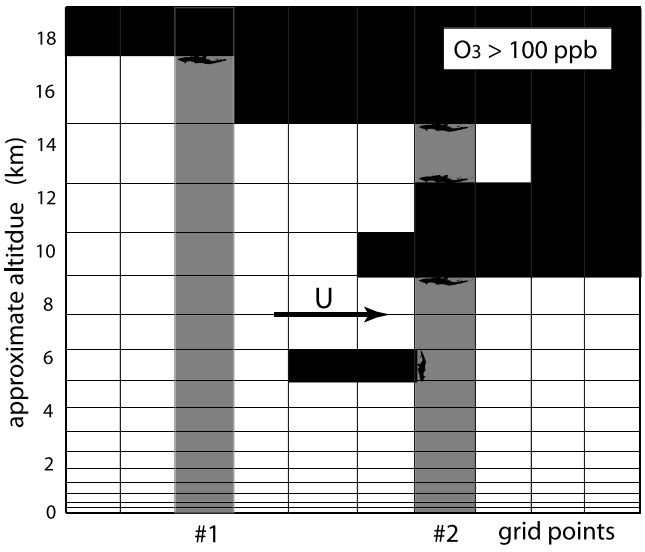

Figure 1. Schematic picture of the type of stratosphere-troposphere boundaries. The stratosphere (solid) is defined by grid boxes having a mean O3 abundance greater than 100 ppb. The mean flow (U) is from left to right. Two tropospheric columns are highlighted (shaded): At grid point 1 the only possible source of stratospheric O3 is from the top (fuzzy solid edge), whereas at point 2 there are four possible surfaces of STE O3 flux.

we can relate the STE ozone flux to atmospheric dynamics. In section 2, the method of diagnosing the STE ozone flux and the model are described. In section 3.1 we present a case study of a westerly duct intrusion of stratospheric O_3 into the tropical troposphere, demonstrating that the model matches the event as observed in column ozone by TOMS. We diagnose the amount of ozone deposited, which is significantly less than calculated simply from the anomalies in the column. In section 3.2 we apply our new diagnostics to two years of meteorological fields and show that the net annual flux is consistent with other empirical estimates, but that the location and timing is counter to some prevailing views, with a larger-than-average flux into the subtropics over much of the year. The geographical distributions of monthly integrated STE for both hemispheres are described. Conclusions and the impact of the cross-tropopause flux on surface O_3 are described in section 4.

2. Model and Methodology

[7] The FRSGC/UCI CTM in this study is driven by the ECMWF Integrated Forecast System (IFS) meteorological data consisting of winds, temperature, convection, precipitation, and boundary layer physics. The original meteorological data are generated at T159 spectral resolution on 40 levels and as 3-hour averages. The CTM runs at a reduced spectral resolution of T63 (~1.9 degrees gridded) or T42 (~2.8 degrees gridded) for these simulations. The original 40-level data are reduced to 37-level for the CTM by combining the lowest 5 levels (0 to 195 m) into 2. The vertical resolution is about 600 m in the troposphere and ~20 mb (a few kilometers) in the middle atmosphere. The model top is 2 mb. The tracer transport uses an updated, vectorized form of the second-order moments algorithm and air mass conservation [*Prather*, 1986; *Prather et al.*, 1987]. Thus, if resolved by the CTM grid (~600 m in the vertical), stratospheric folds will be maintained and are not likely to be mixed into the troposphere by numerical diffusion. Stratospheric ozone is simulated with linearized net photochemical rates (LINOZ [*McLinden et al.*, 2000]). The ozone simulation with full tropospheric chemistry at T63 resolution has been extensively validated against the satellite, ozonesonde, in situ aircraft and lidar observations during TRACE-P period (late February to early April 2001) [*Wild et al.*, 2003, 2004; *Hsu et al.*, 2004]. Stratospheric intrusions are well captured in the model. This success is attributed mostly to the well-simulated stratospheric ozone in the CTM and the ECMWF meteorology.

[8] The LINOZ chemistry scheme operates only in the stratosphere (active down to the defined tropopause to be discussed below), defining production and loss rates that simulate a realistic stratospheric ozone distribution and global mean STE ozone flux of about 550 ± 140 Tg/yr [*Olsen et al.*, 2001]. For computational simplicity, we switch off the tropospheric chemistry, replacing it with a sink in the planetary boundary layer (i.e., the O_3 abundance *e* folds to 20 ppb (parts per billion by mole fraction) in 2 days). Thus every molecule of O_3 in this model originates in the stratosphere, and our fluxes do not include the upward flux of O_3 produced in the troposphere that enters the stratosphere. A back-of-the-envelope calculation of this flux, using the mean residual circulation [*Holton*, 1986] and the tropical upper tropospheric abundance of O_3, gives a reflux of only 10–20 Tg/yr. *Olsen et al.* [2004] show that the net annual global extratropical ozone flux of tropospheric origin is about 22 Tg downward [see *Olsen et al.*, 2004, Table 3], an order of magnitude smaller than the net flux of stratospheric origin. It suggests that ignoring the ozone flux of tropospheric origin would have little impact on the total budget. Because the tropospheric chemical destruction of ozone is simply approximated, and the predicted near-surface ozone abundances should be viewed as qualitative. See *Wild et al.* [2003] for simulations with realistic tropospheric chemistry in which the stratospheric and tropospheric ozone are followed separately.

[9] The objective here is to count a molecule of stratospheric O_3 as having entered the troposphere only when the stratospheric air mass is diluted to tropospheric conditions, so that the O_3 effectively participates in tropospheric chemistry. Thus stratospheric folds and lamina that occur below the traditionally defined, single-valued tropopause [e.g., see *Wei*, 1987, Figure 1] are not counted until the ozone abundance drops below 100 ppb.

[10] Our calculation of ozone fluxes is based on the continuity equation approach, which has been used to derive air mass fluxes [e.g., *Appenzeller and Holton*, 1996]. Instead of the hemispheric budget, we calculate the STE flux into each latitude-by-longitude tropospheric column. To accomplish this, the horizontal tropospheric ozone fluxes must be computed. A tropospheric column with fixed horizontal boundaries aligned to the model grid (e.g., point 1 in Figure 1) will have a varying mass of air and O_3 as the tropopause moves up and down by either horizontal or vertical advection. In Figure 1 stratospheric air masses are defined as having O_3 abundances greater than 100 ppb and

are shaded dark gray. For a given column, the net downward (positive) flux through STE $F_{s\leftrightarrow t}$ can be determined as the residual from computing the other terms in the ozone mass balance as

$$F_{s\leftrightarrow t} = \frac{dM_t}{dt} + F_{t\leftrightarrow t} + S \quad (1)$$

where dM_t/dt is the tropospheric ozone mass change tendency, $F_{t\leftrightarrow t}$ is the net horizontal flux within the troposphere (positive sign for net flux out of the column) and S is the calculated ozone sink (positive by definition) in the lowermost layers. At point 1, the STE ozone flux could also have been computed directly in the CTM from the flux crossing the well defined upper boundary of the troposphere.

[11] In the more general case, such as point 2 in Figure 1, the derivation of the STE O_3 flux is more complex. The net flux at point 1 comes only from erosion of the single tropopause (fuzzy black edge), when O_3 crosses the 100 ppb surface. At point 2, however, the STE flux occurs in four places (fuzzy black edges): the upper most tropopause, on both upper and lower sides of a stratospheric intrusion running across the grid, and on the leading edge of an isolated stratospheric lamina entering the tropospheric column. The advection of high-ozone stratospheric air across the tropospheric column at point 2 around 10 km remains in the stratosphere and should not be counted in the STE O_3 flux. We want to calculate the net flux of O_3 crossing these 4 isopleth surfaces. Thus, in effect, our STE O_3 flux should follow each O_3 molecule and count it when it becomes diluted to "tropospheric" abundance. We must be careful to compute the budget only for the tropospheric air at point 2. The CTM explicitly diagnoses the horizontal fluxes (air and ozone masses per time step) and we separate them into tropospheric and stratospheric by their mean O_3 abundance. While the use of second-order moments in the CTM [*Prather*, 1986] would allow for the calculation of that fraction of a grid box or of an advected parcel that has mean abundance less than 100 ppb, we use only the mean abundance. With this approach, the stratosphere-troposphere boundary is not just a tropopause height, but includes all surfaces that demarcate this boundary. Because we have turned off tropospheric chemistry, we cannot misdiagnose high-ozone tropospheric pollution events as stratospheric.

[12] A similar approach might use a potential vorticity (PV) isopleth, such as 2 PVU, to define the tropopause. In our simulations, the PV distribution at the 2 PVU surface is similar to 100 ppb surface (e.g., see Figure 3) but is more noisy because of the creation of tropospheric high PV, e.g., by radiative cooling near high-latitude surfaces. Selecting the tropopause as an isopleth surface of potential vorticity or ozone is a consistent definition and is commonly used and allows for multiple, unconnected stratospheric regions. Since we have no chemistry in this region, it does not matter if the tropopause is more like a transition layer [*Pan et al.*, 2004].

[13] T42 meteorological data for two different years (May 2000 to April 2001 and January to December 1997) are used. For each simulation the CTM is spun up to a near steady state by repeating the same annual meteorological data for 5 years. In addition, for the TRACE-P period (November 2000 to April 2001), we have higher-resolution T63 met fields. For convenience, a lower–horizontal resolution T21 version of the same meteorological field is used to spin up the stratospheric ozone and initialize the T63 run. We find similar monthly latitude-longitude STE fluxes and the differences in the zonal mean fluxes are in general well within 10%. For the case study of a westerly duct during March 2001 (section 3.1), T63 meteorology data are used.

3. Results

[14] In section 3.1 we apply our STE ozone flux diagnostics to a deep stratospheric intrusion that occurred in a westerly duct in the tropical Pacific during March 2001. We analyze this event because it is seen clearly in the TOMS satellite data and overlaps with our more extensive analysis during the TRACE-P mission. The amount of ozone mixed into the troposphere is compared with the anomalous burden observed by TOMS. We contrast the cross-tropopause flux of ozone occurring via this westerly duct in the east Pacific region with the flux into the quiet west Pacific region during the same period.

[15] The global analysis of the STE is described in section 3.2. We discuss the annual cycle of the hemispheric O_3 STE for both years and the monthly zonal budgets of the tropospheric ozone columns are presented. The smooth zonal STE distributions is then compared to the more noisy latitude-longitude monthly STE maps and the seasonal migration of these patterns along with the zonal wind at 200 mb are shown. The meteorological processes leading to the O_3 STE are then identified. Data from year 2000/2001 are used to illustrate the seasonal cycle but the monthly STE distributions for 1997 are qualitatively similar. The main differences between these two years are discussed separately, where the STE associated with the El Nino winter month (December 1997) is contrasted with that of the La Nina winter month (December 2000). The difference between May 2000 and May 1997 is also notable. We find the Tibetan Plateau in May of both years to be the location of intense ozone flux associated with the rapid tropopause rising during the spring time.

3.1. Deep Tropical Intrusion Through the Westerly Duct: A Case Study in March 2001

[16] The climatology of stratospheric intrusions into the tropical troposphere within the westerly ducts, defined by potential vorticity and ozone, has been extensively studied [*Waugh and Polvani*, 2000; *Waugh and Funatsu*, 2003]. The tropical troposphere is characterized by very low ozone abundances (<30 ppb) with layers of high ozone (>60 ppb) attributable to biomass burning plumes or stratospheric intrusions [e.g., *Fenn et al.*, 1999; *Browell et al.*, 2001]. In addition to these studies characterizing high-O_3 with high-PV in the tropics, there is clear statistical evidence that stratospheric intrusions reach along isentropes into the deep tropical troposphere [e.g., *Hsu et al.*, 2004, Figure 3]. Here we seek to quantify the amount of ozone brought into the tropical troposphere by a single intrusion event over the east Pacific in March 2001.

[17] Figure 2 shows the total ozone columns from TOMS swath data for 13, 14, and 15 March 2001 and the corresponding CTM T63 full-chemistry simulations taken

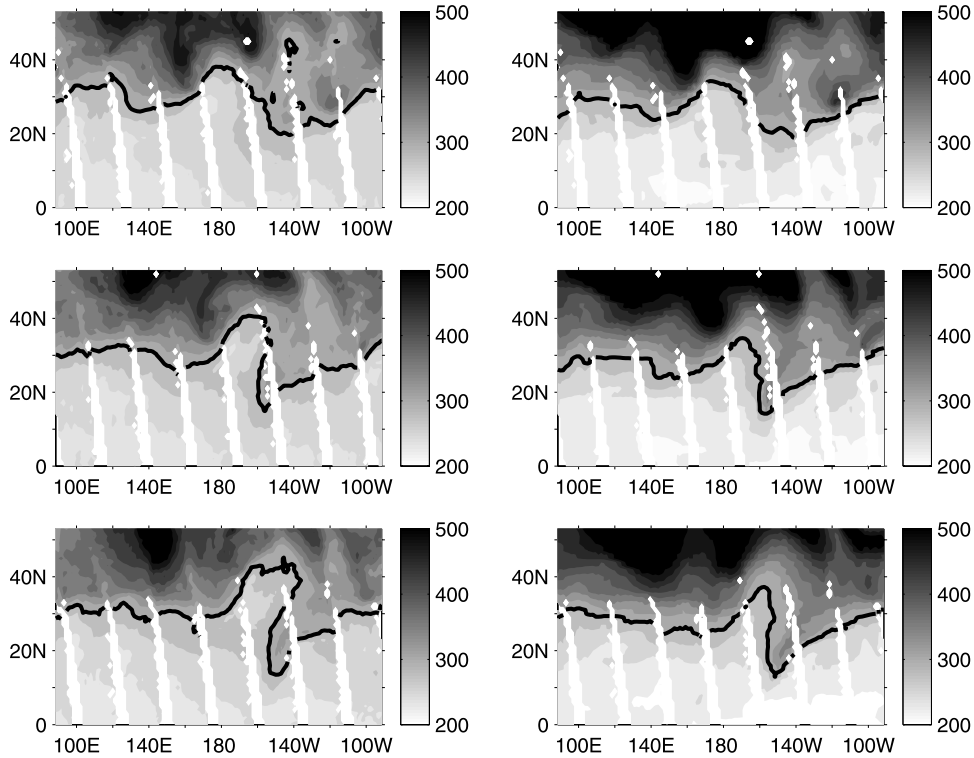

Figure 2. Total ozone columns in Dobson units for 13–15 March 2001 (top to bottom) with orbits starting from 16 GMT from the eastmost of the domain to 5 GMT to the westmost of the domain. (left) TOMS swath data. (right) Concurrent CTM simulations. The 300 DU contours are emphasized with bold solid lines.

from *Wild et al.* [2003]. In comparison with the observation, the CTM captures realistic variations but with a larger latitudinal gradient with total ozone column biased high in the north and low in the tropics. The anomaly becomes apparent on 14 March (Figure 2, second panel) when the 300 Dobson Unit contour lines near 150°W extend southward, reaching to 15°N on 16 March (Figure 2, third panel). The timing, magnitude, and pattern of this event are matched in the CTM simulation (Figure 2, right).

[18] The three-dimensional nature of this intrusion is shown in the CTM simulation of PV and O_3 fields on the 330K potential temperature surface for 13, 15, and 17 March (Figure 3). The 330 K isentrope slopes downward from the stratosphere at the subtropics into the midtroposphere in the deep tropics (not shown). In the CTM both PV and O_3 fields show qualitatively similar distributions with a thin tongue intruding into the tropics through the westerly duct, which is enclosed by the zero wind lines (dashed white lines). Between 15 and 17 March, the high-PV strip on the 330K isentrope rolls up and breaks away from the stratosphere, with parallel evolution of the high-O_3 air. This apparently isolated blob of high PV and O_3 near 10°N–20°N and 150°W slowly drifts to the north and much of the material appears to merge back into the stratosphere on 19 March (not shown). During this same period, the tropical west Pacific is relatively quiet.

[19] The individual terms in the continuity equation for tropospheric ozone over the northern tropical Pacific (0–23°N, 90°E–90°W) are shown in Figure 4. Figures 4a–4c show the ozone diagnostics from equation (1) for 24-hour period 0000–2400 UT 14 March 2001: (Figure 4a) tropospheric ozone mass change (dM/dt); (b) tropospheric flux divergence($F_{t\leftrightarrow t}$); and (c) STE flux ($F_{s\leftrightarrow t}$). Contour intervals are regular at ±10 g-O_3 m^{-2} y^{-1}. For comparison, the global average STE flux is 1.0 g-O_3 m^{-2} y^{-1}. The near-surface sink (S, not shown) is similar in magnitude to the global average and would not appear at this contouring level. Because of the numerical approximations noted earlier (i.e., we count air masses as either stratospheric or tropospheric on the basis of their mean ozone abundance and do not interpolate fractional volumes), the accumulated STE flux for a single day is noisy and includes dipole-like features with unrealistic negative values.

[20] The tropospheric ozone mass shows a large negative change as the stratospheric intrusion displaces the tropospheric air. This is matched by the large, compensating flux divergence term. The STE flux indicates that for 14 March there has not yet been significant mixing of ozone into the troposphere. The 3-day sequence of STE flux for 14–16 March continues with Figures 4c–4e. The major contribution to the STE flux is seen on 15 March in Figure 4. The STE has a maximum near the end of the event on 16 March, and it is located about 160°W and 5°N, deep in the tropics where the stratospheric ozone is finally mixed into the troposphere. Analysis of this CTM simulation shows that the majority of the high-PV/high-O_3 intrusion returns to the stratosphere, and thus the STE flux cannot be estimated simply from the mass of O_3 in

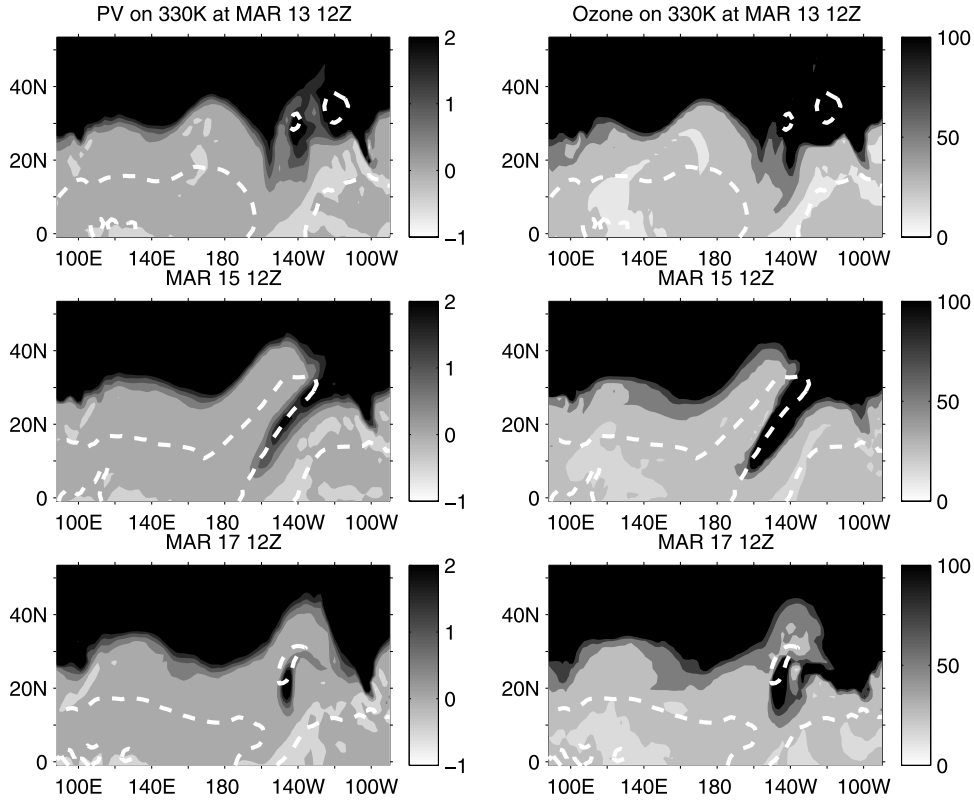

Figure 3. (left) Potential vorticity on 330K in PV units (1 PVU = 10^{-6} K m^2 kg^{-1} s^{-1}) for 13, 15, and 17 March 2001 at 12Z. (right) Concurrent ozone distributions on 330K (in ppb). The dashed lines represent the zero-wind lines.

the tongue of stratospheric air, or from the anomaly in the column O_3.

[21] The STE ozone flux, averaged over the western (dashed line) and eastern half (solid line) of the north tropical Pacific basin (90°E–90°W, 0°–20°N), is shown in Figure 5. These fluxes can be compared with the global, annual average of 1.0 g-O_3 m^{-2} y^{-1} and are calculated from the CTM's 3-hour diagnostics for 13–20 March 2001. The eastern basin shows clearly elevated STE ozone fluxes greater than 2.5 g-O_3 m^{-2} y^{-1} for about 48 hours on days 15–17. Although the event starts on the 14th, the peak flux does not occur until midday of the 15th. The flux remains high until the 17th. We can estimate the additional STE flux due to this event as about 0.3 Tg of ozone. This number is much smaller than 1.7 Tg, the integrated anomaly relative to the monthly median pattern, seen in TOMS total column ozone over the same domain on 15 March. Indeed, only a small fraction of the intrusion is diluted into the troposphere.

3.2. Global Distributions: Year 1997 and Year 2000/2001

3.2.1. Annual Cycle

[22] The global STE flux is about 550 Tg-O_3 (1.07 g-O_3 m^{-2} y^{-1}) and 515 Tg-O_3 (1.00 g-O_3 m^{-2})for years 2000/2001 and 1997, respectively. For both years, the ozone flux is split evenly to within 5% between the Northern Hemisphere (NH) and Southern Hemisphere (SH). Both the magnitudes and the partition of ozone fluxes between hemispheres are similar to the results of *Olsen et al.* [2004] (see their Table 2) even though their budget excludes the contribution of ozone flux from the tropics and our calculation does not include the ozone flux of tropospheric origin. Figure 6 shows the monthly STE ozone flux (expressed in units of Tg-O_3 y^{-1}) for both NH and SH. The net ozone flux exhibits similar patterns for both years: namely, the largest STE fluxes occur in late spring/early summer; and the smallest, in autumn through early winter. These seasonal patterns can be directly compared to the net ozone flux of stratospheric origin shown by *Olsen et al.* [2004, Figure 2]. In their study, the net NH ozone flux of stratospheric origin has a similar but much broader distribution with maximum downward fluxes in March through July. Note that their result is from a 5-year mean and hence much of the interannual variability is averaged out. In Figure 6, the SH ozone flux shows much less seasonal variation than the NH flux, also in agreement with *Olsen et al.* [2004]. The SH ozone reaches its maximum in the austral spring to early summer (SOND) as shown. In the work by *Olsen et al.* [2004], the SH downward ozone flux of stratospheric origin shows a similar distribution but with a more distinct maximum in September.

[23] Comparing the two different years, we find that the NH seasonal variation is much larger for year 2000/2001 but has the same annual total. The SH seasonality changes little, but the total amount in year 1997 is 10% less than in year 2000/2001. In the next section,

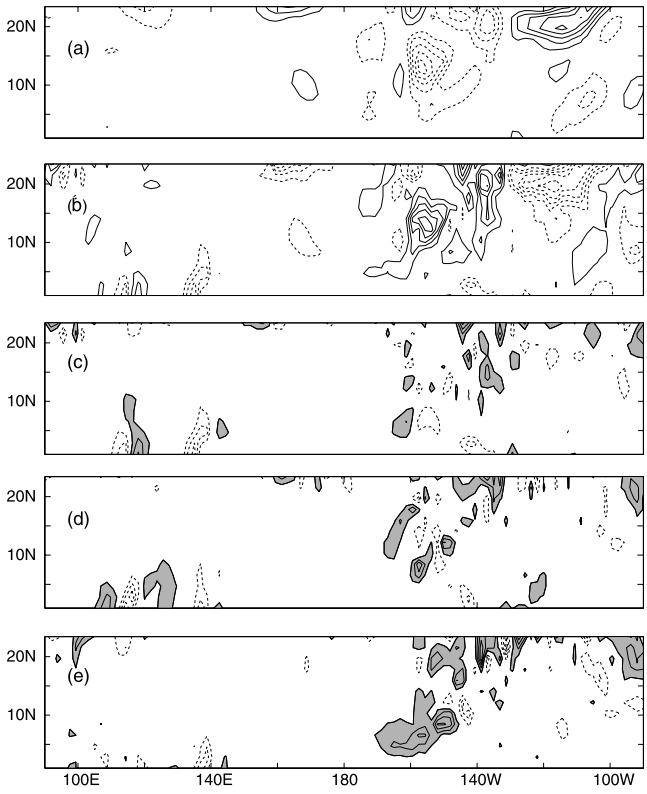

Figure 4. (a) Tropospheric ozone column mass tendency (dM_t/dt) for 14 March 2001. (b) Net horizontal tropospheric flux ($F_{t\leftrightarrow t}$) for 14 March 2001. Net STE flux ($F_{s\leftrightarrow t}$) for (c) 14 March, (d) 15 March, and (e) 16 March 2001. All quantities are in units of g-O_3 m^{-2} y^{-1}. Positive (negative) values are in solid (dashed) lines. The contour interval is 10. For Figures 4c–4e, absolute values greater than 10 are shaded.

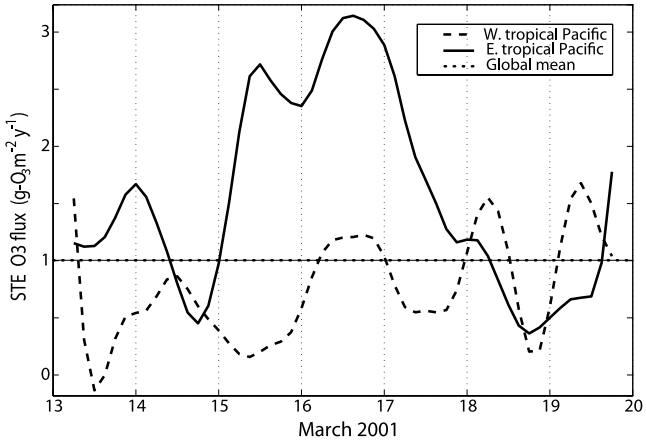

Figure 5. STE flux in units of g-O_3 m^{-2} y^{-1} over West Pacific (dashed line) and East Pacific (solid line) from 13–20 March 2001. The horizontal dashed line is the global average for year 2000/2001.

we focus on year 2000/2001 since the distribution of STE of ozone is qualitatively similar for both years.

3.2.2. Latitudinal Distributions of Monthly STE Distributions

[24] Figure 7 shows the zonal mean tropospheric ozone budgets accumulated over the months of April 2001 and October 2000. All four terms in equation (1) are plotted in units of g-O_3 m^{-2} y^{-1} versus sine latitude: the STE flux, $F_{s\leftrightarrow t}$ (solid line); the surface sink, S (dotted); the mass tendency, dM/dt (dot-dashed); and the tropospheric flux divergence, $F_{t\leftrightarrow t}$ (dashed). When averaged over longitude and a month, the first two of these terms dominate, in contrast to the daily maps where the latter two dominate (see Figure 4). The mass tendency term oscillates, being positive in the spring hemisphere and negative in the fall hemisphere. The near-surface sink shows a broad distribution with maxima shifted equatorward of the STE flux, indicating general tropospheric transport of stratospheric ozone toward the tropics. Our simplified sink, with uniform loss frequency in the lowest model layers, exaggerates the loss of stratospheric ozone at high latitudes where ozone photodestruction will be much less than in the tropics, especially during winter. Thus these results underestimate the transport of ozone of stratospheric origin into the tropics and in reality the sink should be shifted even more equatorward.

[25] The geographic location of the STE O_3 flux for several months is shown in Figure 8. In these latitude-by-longitude plots of monthly mean STE, the colored contours show regions of positive and negative STE (g-O_3 m^{-2} y^{-1}); the monthly mean zonal wind at layer 29 (about 200 hPa) is contoured in thin black lines at intervals of ±10, 30, and 50 ms^{-1}; and the zero-wind line is emphasized by the thick dash-dot contour. One can compare the relatively smooth, zonal mean STE (Figure 7) with the longitudinal variations of positive and negative STE seen in Figure 8. These large negative (upward) STE are unrealistic except in deep tropics and due to the numerical limitation of our ability to accurately diagnose the zonal transport of "tropospheric" ozone.

[26] We can identify the cause of this noise as follows, but have no easy fix. In the presence of large zonal winds

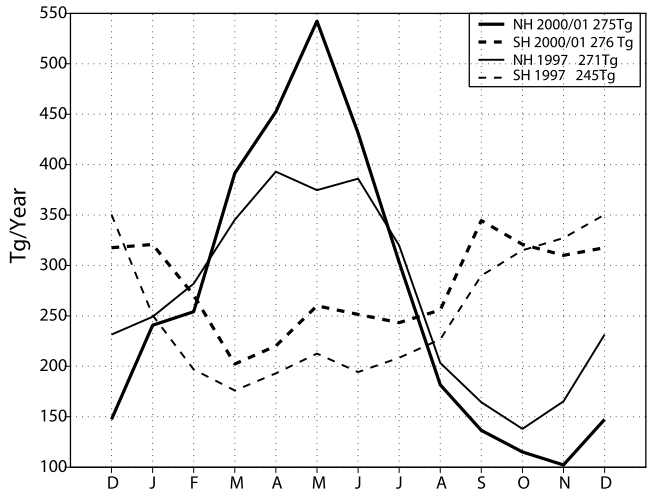

Figure 6. Monthly STE in units of Tg/year for Northern (solid lines) and Southern hemispheres (dashed line). The thick lines are for year 2000/2001, and thin lines are for year 1997.

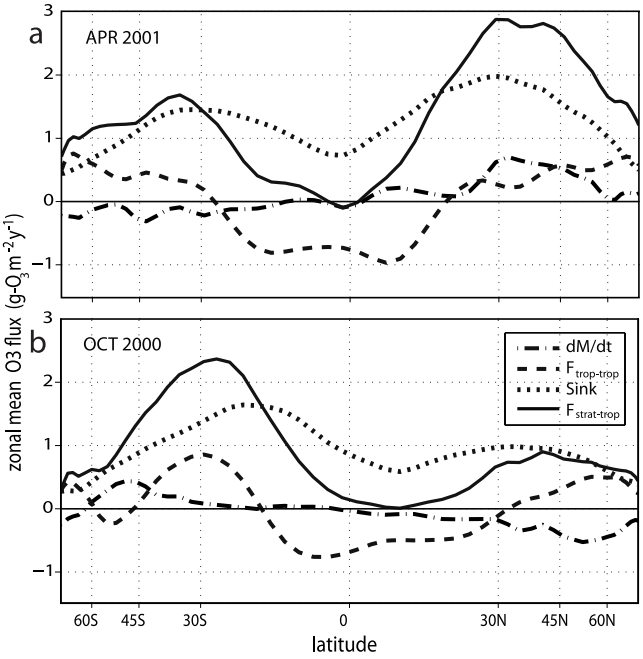

Figure 7. Zonal budget for tropospheric ozone columns for (a) April 2001 and (b) October 2000.

and gradients in ozone near the 100 ppb isopleth, the westerly flow advects air masses containing both stratospheric and tropospheric air (defined by the 100-ppb surface) within a grid box. This mixed parcel will be transported in the CTM with the mixture preserved by the second-order moments advection algorithm, but our diagnosed flux will put all of the ozone into either stratospheric or tropospheric flux on the basis of the mean ozone abundance. Errors will accumulate, and since ozone is conserved they will appear as equal terms of opposite sign in neighboring regions. For example, along the winter jet stream the errors are largest.

3.2.3. Correlation of Ozone Flux and Meteorological Events

[27] Figure 8a shows the STE distributions for January 2001. For boreal winters (DJF), intense STE is expected to follow the jet streams where folds and cut-off lows take place both in Asia/Pacific and Atlantic regions, although this picture is much obscured by the noise level seen as the dipole structures in Figure 8a. Other notable features include regions of positive STE spread north to higher latitudes over the exit region of the Pacific jet stream and the North America continent. The intense dipoles within the Pacific jet stream and at the poles cancel and result in a fairly weak zonal contributions of winter STE to the global budget (e.g., for January 2001, the zonal average flux decreases from 1.4 g-O_3 m^{-2} y^{-1} at 30°N to less than 0.9 for 60°N–90°N). Our noisy patterns look qualitatively similar to the cross-tropopause air mass flux presented by *Gettelman and Sobel* [2000, Figure 5] in which dipole structures are prevalent. While these dipole structures in the cross-tropopause flux may be real for air mass, our results should not be taken as evidence for them. Even if the air flow were to include such in-out fluxes, the ozone flux should be predominantly downward because of the large difference in O_3 mixing ratio. In the months of February 1997 (not shown) and January 2001, the regions of large STE dip into the deep tropics through the middle and eastern Pacific regions where the westerly ducts are located. For these two months, the estimated zonal STE is elevated at 10°N (about 0.5 g-O_3 m^2 y^{-1} whereas in typical winter months when no apparent intrusion signatures are seen, the STE flux is deep tropics is nearly 0 or negative (upward). The existence of a westerly duct in the monthly mean flow, however, does not guarantee large STE fluxes.

[28] In NH spring, the STE patterns move southward out of the jet stream regions. Figure 8b shows STE distributions for March 2001. For March, the pattern still resembles wintertime, but the positive fluxes are intensified and broadened with latitude. Two factors may explain this intensification of the March STE: (1) the buildup of lower-stratospheric ozone over the winter and (2) the strengthening, as compared to midwinter, of upper troposphere baroclinic activity for the Pacific jet stream [*Nakamura*, 1992]. In April 2001 (Figure 8c) an intense STE pattern appears around the subtropical Tibetan Plateau and reaches its maximum in May 2000 (Figure 8d). This pattern weakens and extends northward and eastward to China in June (not shown). In May 2000 (and also in May 1997, not shown) the STE are most intense around the 20°N–40°N latitudinal belt. This is apparently associated with the transition of the subtropical jet moving poleward and the rise of the tropopause on the anticyclonic side of the jet [see *Robinson*, 1980, Figure 1]. Indeed, *Appenzeller and Holton* [1996] show that the maximum STE in NH late spring are associated with the rapid rise of the tropopause, primarily around 25°–40°N. More detailed analysis of the Tibetan Plateau is given in section 3.2.5.

[29] In NH summer, the jet streams move northward to 40°N–45°N, as do the STE distributions, and STE is mostly dominant over the continents as shown for July 2000 (Figure 8e). This pattern is in agreement with most of the previous studies. The maximum over the subtropical west Pacific region appears in April and continues until August. This local subtropical STE maxima overlaps with the weak westerlies (<10 ms^{-1}) and coincides with the locations for frequent breaking of quasi-stationary Rossby waves [*Postel and Hitchman*, 1999; *Abatzoglou and Magnusdottir*, 2004]. *Jing et al.* [2004] find that the ozone flux along isentropes between 330–370K occurs preferentially over the subtropical Atlantic and Pacific oceans during the summer when this wave breaking occurs. In autumn the NH STE is at its minimum and gradually shifts off the continents back to the oceans (see Figure 8f for September 2000).

[30] The SH distributions of STE show less pronounced zonal variations in Figure 8 as expected from the general lack of land-sea contrast. Another contrast with the NH is that regions of peak STE remains predominantly in the subtropical region (20°S–35°S) even as the zonal jet moves to higher latitudes in the summer. It suggests that isentropic mixing in the subtropics is the more dominant SH pathway for STE exchange, even in summer.

3.2.4. Interannual Variations, an ENSO Year

[31] For the two years analyzed here, December 1997 (Figure 8h) is in the warm phase of ENSO (El Nino), whereas December 2000 (Figure 8g) is in the cold phase of ENSO (La Nina). For December 1997, there is no

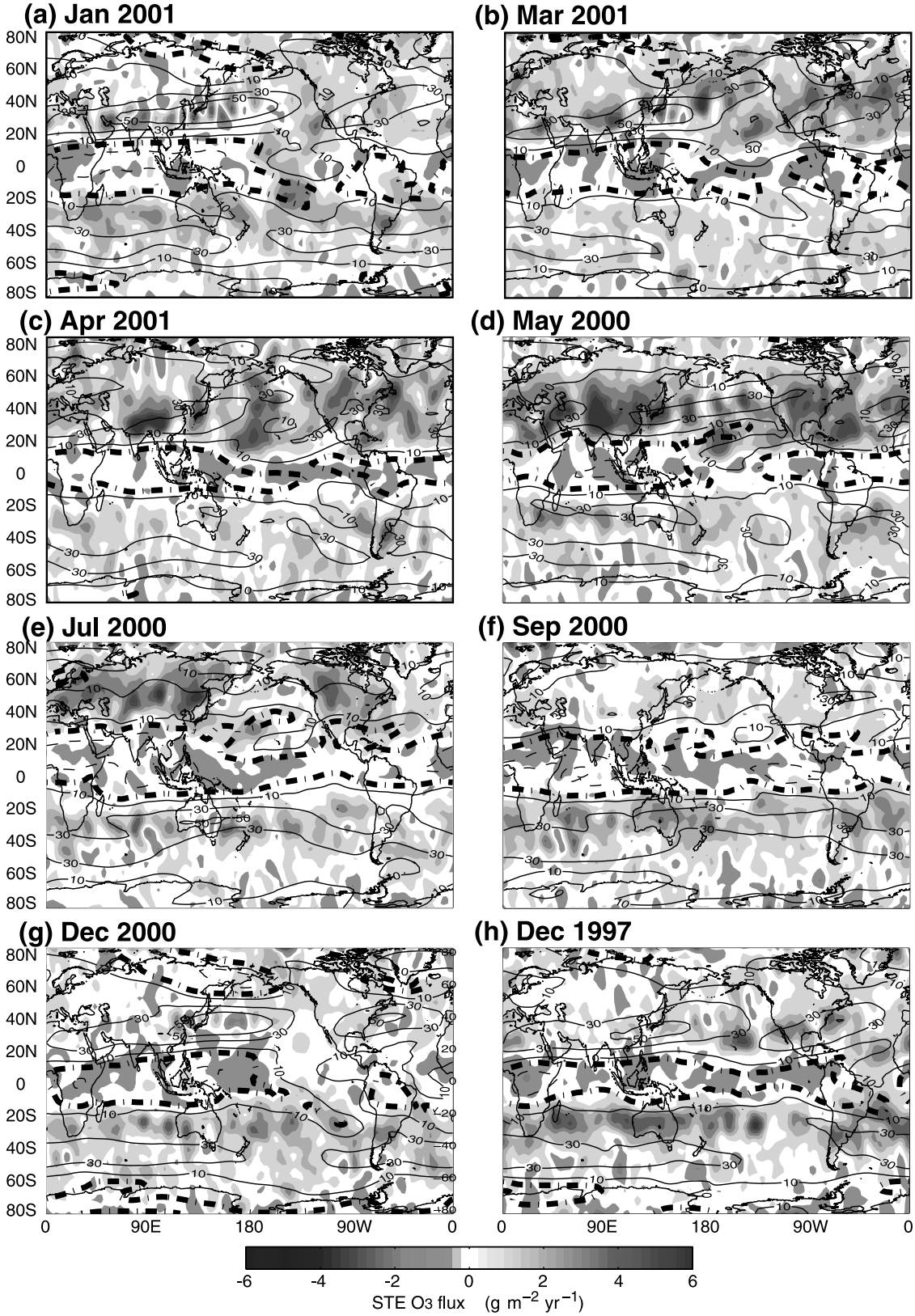

Figure 8. Color contours of monthly latitude-longitude STE flux in units of g-$O_3 m^{-2}$ y^{-1}. The color contour interval is 1. The thin solid (dashed) lines are the contours of the zonal winds (ms^{-1}) at 200 mb. The contour levels are ±10, 30, and 50. The zero wind lines are emphasized in bold dashed lines. See color version of this figure at back of this issue.

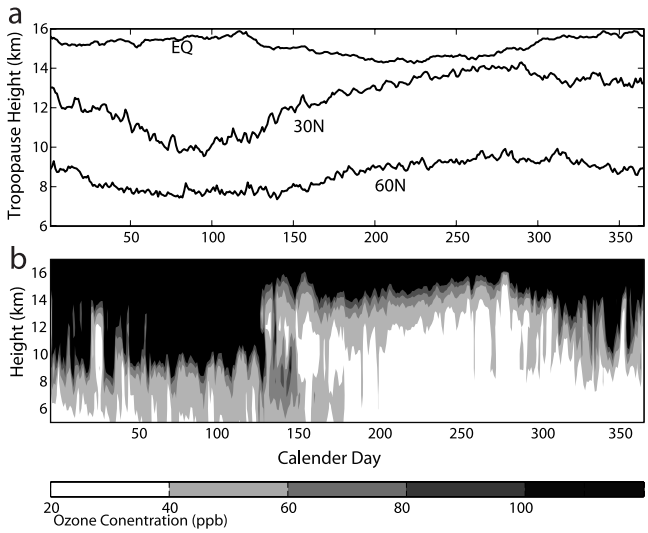

Figure 9. (a) Zonal mean tropopause height as a function of the calendar day at equator, 30°N and 60°N for year 2000/2001 data. (b) Ozone mixing ratio in ppb averaged over 80°–100°E (Tibetan plateau) at 30°N as a function of pressure height and calendar days for year 2000/2001. The contour interval is 20 ppb.

westerly duct in the Pacific Ocean and the NH zero-wind line recedes toward the equator in the East Pacific. Also, the jet stream over North America is tilted further equatorward at the entrance region. The accompanying STE is large along the North America/Atlantic jet stream, as compared to that in December 2000. As a result, the zonal mean STE for December 1997 has a maximum ($\sim$1.9 g-O_3 m^{-2} y^{-1}) at 25°N, south of the zonal mean zonal jet, while in December 2000 the zonal mean STE distribution in NH is uniformly flat and weak ($\sim$0.6 g-O_3 m^{-2} y^{-1}). The difference in the total NH wintertime flux for the two years is also apparent in Figure 6. Similar interannual variability due to ENSO has been found in observations [*Langford*, 1999].

[32] In Figure 6, however, the most obviously different month is May. For May 1997, the STE distributions have similar patterns, as shown for May 2000 in Figure 8d with a distinct and large influx over the Tibetan Plateau and with other lesser maxima occurring in the same latitudinal belt (20°–45°N). The major difference between the two years is from the overall magnitude of the flux. Changes in the stratospheric column of ozone cannot readily explain the difference in STE, since the column ozone from 10°N to 50°N is identical to within 5% for the two years (not shown). Therefore the most likely causes are meteorological conditions: in May 2000, the vertical and horizontal wind shear in the upper troposphere are much stronger than that in May 1997. Stronger instability might be the cause for more effective STE; however, establishing a quantitative link between the instability and ozone flux is beyond our current study.

3.2.5. Large Flux Over the Tibetan Plateau

[33] Figure 9a shows the effective zonal mean tropopause height for the equator, 30°N and 60°N as a function of calendar day. The pressure altitude (z*) at each longitude is determined by the first altitude (from the top down) at which the stratospheric O_3 abundance drops below 100 ppb. The z* are then averaged zonally. Results are shown for the EC met fields year 2000/2001. In contrast with the equator and at 60°N, there is a large seasonal cycle at 30°N, with a particularly rapid rise during boreal spring (days 100–150).

[34] Over the Tibetan Plateau (30°N, 80°E–100°E), a more dramatic lifting of the boundary between stratosphere and troposphere can be seen in Figure 9b. The gray scale shows contours of O_3 abundances of 20, 40, 60, 80 and 100 ppb, again as a function of calendar day. In winter and spring the tropopause is very close to the plateau and the influence of stratospheric ozone on surface abundances should be large. In the summer and autumn the tropopause is more remote and the stratospheric influence at the surface should be minimal. Around Day 130 (early May) the 100-ppb boundary rises suddenly from 9–10 km to 15 km. Note that at the break point in our meteorological year, 1 May, there is no obvious discontinuity in O_3. In the following month, there are exceptionally high ozone abundances in the troposphere, consistent with the very large STE flux shown in Figure 8d. The enhanced STE O_3 flux over the Tibetan Plateau is not a numerical artifact of the hybrid coordinate system in the atmospheric model, but clearly related to a rapid rise in the tropopause associated with the transition of the subtropical jet [*Robinson*, 1980]. Analysis for the year 1997 likewise shows a clear disruption of the tropopause from calendar day 130 on with rapidly alternating summer and winter tropopauses before settling to the summer tropopause around day 160. During this transition period, a substantial quantity of stratospheric ozone is mixed into the troposphere. We suggest that elevated surface heating in the late spring makes the Plateau a hot spot for STE exchange.

4. Conclusions

[35] We present a new method for diagnosing the flux of stratospheric ozone into the troposphere that is based on the continuity equation for the column of tropospheric O_3. The flux of stratospheric ozone is diagnosed only when the stratospheric air has mixed down to tropospheric abundances and hence participates in tropospheric chemistry. This flux is conserved and would give the same global, annual mean as that computed by the flux crossing a pressure surface in the upper troposphere, but it gives more accurate information on where and when the ozone becomes tropospheric.

[36] The latitude-by-month patterns of our diagnosed STE O_3 flux for 1997 (515 Tg-O_3 per year) and 2000/2001 (550 Tg-O_3 per year) are shown in Figure 10. The two years are not very different. The annual flux is consistent with other estimates. Both years show a NH with significant subtropical influx most of the year, but with midlatitude influx important only in spring and summer and peaking in May. Both years show an equally large SH flux with much less seasonality and peak fluxes about 30°S. Surprisingly, high latitudes are not a significant region of STE, even on a per area basis.

[37] In general the fate of the STE ozone flux is to travel further downward in altitude and equatorward where it is destroyed by photochemistry or surface uptake. This shift is seen in our simulation as isentropic descent to a uniform

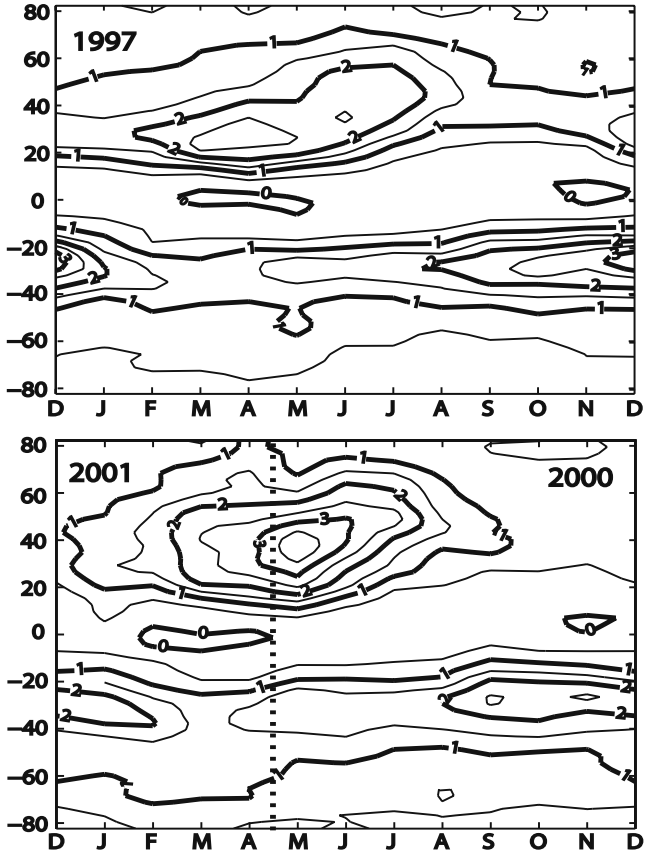

Figure 10. STE flux in units of g-O_3 m^{-2} y^{-1} as a function of latitude and month for (top) year 1997 and (bottom) year 2000/2001.

loss frequency in the lowest layers. If we had included realistic tropospheric chemistry, we would expect this equatorward shift of the sink to be greater since the tropics are more chemically active.

[38] How would these fluxes of stratospheric ozone influence the abundance of tropospheric ozone? The source of the springtime ozone maximum at the surface remains an unresolved issue [e.g., *Monks*, 2000]. We cannot directly use our modeled surface abundances, since our uniform chemical loss frequency does not have the right latitudinal and seasonal variation. To first order we might expect the largest impact of stratospheric ozone in the subtropics where the flux is consistently large year-round. The SH impact would be more uniform throughout the year, but the NH would show large stratospheric influence during May-June at midlatitudes but not polar regions. If we factor in more realistic photochemical destruction of ozone (i.e., negligible at mid and high northern latitudes until late spring), the stratospheric ozone would accumulate during winter and peak in spring. It is possible that this seasonality, with ozone destruction becoming more rapid by May-June drives the peak abundances to early spring. Similarly, without loss at high latitudes in winter, even small STE fluxes would accumulate, producing a maximum contribution over the poles in order to drive a flux to the lower-latitude sink.

[39] Our results differ greatly from those of *James et al.* [2003] who found that the "deep" air STE has a distinct winter maximum. The calculated STE in this study is also effectively "deep" since our calculation shows that the latitude-by-month STE distributions correlate well with tropospheric ozone concentrations from the surface to about 600 mb with an correlation coefficient >0.6. Even varying ozone loss rates, James et al. could not obtain a late spring ozone maximum for the lower altitudes. In contrast, in our calculations the STE O_3 flux drives a spring maximum in tropospheric O_3.

[40] The results shown here are limited to one type of meteorological field: the European Centre's IFS 40-level pieced forecasts derived by U. Oslo. They are also restricted to an artificial simulation that includes only stratospheric chemistry, and hence every ozone molecule originated in the stratosphere. This simplified chemistry, however, allows us to more accurately diagnose the when and where of stratosphere-to-troposphere ozone flux. Tropospheric ozone simulations using the same met fields with full tropospheric chemistry [*Wild et al.*, 2003] can be used to relate these fluxes to estimates of the stratospheric influence on tropospheric ozone abundances. The more practical questions, e.g., how stratospheric ozone depletion has altered tropospheric ozone, cannot be answered by this work or by simply tagging ozone molecules in a CTM. They require a fully coupled simulation of both stratospheric and tropospheric chemistry before and after the rise of halocarbons.

[41] **Acknowledgments.** Juno Hsu is currently supported by The Gary Comer Abrupt Climate Change Fellowship. The authors are grateful to the NASA/GSFC TOMS Ozone Processing Team for access to the TOMS ozone column products.

References

Abatzoglou, J. T., and G. Magnusdottir (2004), Nonlinear planetary wave reflection in the troposphere, *Geophys. Res. Lett.*, *31*, L09101, doi:10.1029/2004GL019495.

Appenzeller, C., and J. R. Holton (1996), Seasonal variation of mass transport across the tropopause, *J. Geophys. Res.*, *101*, 15,071–15,078.

Brewer, A. M. (1949), Evidence for a world circulation provided by the measurements of helium and water vapor distribution in the stratosphere, *Q. J. R. Meteorol. Soc.*, *75*, 351–363.

Browell, E. V., et al. (2001), Large-scale air mass characteristics observed over the remote tropical Pacific Ocean during March–April 1999: Results from PEM-Tropics B field experiment, *J. Geophys. Res.*, *106*(D23), 32,481–32,502.

Chen, P. (1995), Isentropic cross tropopause mass exchange in the extratropics, *J. Geophys. Res.*, *100*, 16,661–16,673.

Danielsen, E. F. (1961), Trajectories: Isobaric, isentropic and actual, *J. Atmos. Sci.*, *18*(4), 479–486.

Dethof, A., A. O'Neill, and J. Slingo (2000), Quantification of the isentropic mass transport across the dynamical tropopause, *J. Geophys. Res.*, *105*, 12,279–12,293.

Fenn, M. A., et al. (1999), Ozone and aerosol distributions and air mass characteristics over the South Pacific during the burning season, *J. Geophys. Res.*, *104*(D13), 16,197–16,212.

Gettelman, A., and A. H. Sobel (2000), Direct diagnoses of stratosphere-troposphere exchange, *J. Atmos. Sci.*, *57*, 3–16.

Hall, T. M., and M. Holzer (2003), Advective diffusive mass flux and implications for stratosphere-troposphere exchange, *Geophys. Res. Lett.*, *30*(15), 1826, doi:10.1029/2003GL017745.

Holton, J. R. (1986), Meridional distribution of stratospheric trace constituents, *J. Atmos. Sci.*, *43*, 1238–1242.

Holton, J. R., P. H. Haynes, M. E. McIntyre, A. R. Douglass, R. B. Rood, and L. Pfister (1995), Stratosphere-troposphere exchange, *Rev. Geophys.*, *33*, 403–439.

Hsu, J., M. J. Prather, O. Wild, J. K. Sundet, I. S. A. Isaksen, E. V. Browell, M. A. Avery, and G. W. Sachse (2004), Are the TRACE-P measurement representative of the western Pacific during March 2001?, *J. Geophys. Res.*, *109*, D02314, doi:10.1029/2003JD004002.

James, P., A. Stohl, C. Forster, S. Eckhardt, P. Seibert, and A. Frank (2003), A 15-year climatology of stratosphere-troposphere exchange with a La-

grangian particle dispersion model: 2. Mean climate and seasonal variability, *J. Geophys. Res.*, *108*(D12), 8522, doi:10.1029/2002JD002639.
Jing, P., D. M. Cunnold, H. J. Wang, and E.-S. Yang (2004), Isentropic cross-tropopause ozone transport in the Northern Hemisphere, *J. Atmos. Sci.*, *61*, 1068–1078.
Kiley, C. M., et al. (2003), An intercomparison and evaluation of aircraft-derived and simulated CO from seven chemical transport models during the TRACE-P experiment, *J. Geophys. Res.*, *108*(D21), 8819, doi:10.1029/2002JD003089.
Langford, A. O. (1999), Stratosphere-troposphere exchange at the subtropical jet: Contribution to the tropospheric ozone budget at midlatitudes, *Geophys. Res. Lett.*, *26*(16), 2449–2452.
Logan, J. A. (1999), An analysis of ozonesonde data for the troposphere: Recommendations for testing 3-D models and development of a gridded climatology for tropospheric ozone, *J. Geophys. Res.*, *104*(D13), 16,115–16,150.
Logan, J. A., et al. (1999), Trends in the vertical distribution of ozone: A comparison of two analyses of ozonesonde data, *J. Geophys. Res.*, *104*(D21), 26,373–26,400.
McLinden, C. A., S. C. Olsen, B. J. Hannegan, O. Wild, and M. J. Prather (2000), Stratosphere ozone in 3-D models: A simple chemistry and the cross-tropopause flux, *J. Geophys. Res.*, *105*(D11), 14,653–14,666.
Monks, P. S. (2000), A review of the observations and origins of the spring ozone maximum, *Atmos. Environ.*, 3545–3561.
Murphy, D. M., and D. W. Fahey (1994), An estimate of the flux of stratospheric reactive nitrogen and ozone into the troposphere, *J. Geophys. Res.*, *99*(D3), 5325–5332.
Nakamura, H. (1992), Midwinter suppression of baroclinic wave activity in the Pacific, *J. Atmos. Sci*, *49*, 1629–1642.
Olsen, S. C., C. A. McLinden, and M. J. Prather (2001), Stratospheric N_2O-NO_y system: Testing uncertainties in a three-dimensional framework, *J. Geophys. Res.*, *106*, 28,771–28,784.
Olsen, M. A., A. R. Douglass, and M. R. Schoeberl (2002), Estimating downward cross-tropopause ozone flux using column and potential vorticity, *J. Geophys. Res.*, *107*(D22), 4636, doi:10.1029/2001JD002041.
Olsen, M. A., M. R. Schoeberl, and A. R. Douglass (2004), Stratosphere-troposphere exchange of mass and ozone, *J. Geophys. Res.*, *109*, D24114, doi:10.1029/2004JD005186.
Pan, L. L., W. J. Randel, B. L. Gary, M. J. Mahoney, and E. J. Hintsa (2004), Definition and sharpness of the extratropical tropopause: A trace gas perspective, *J. Geophys. Res.*, *109*, D23103, doi:10.1029/2004JD004982.
Plumb, R. A. (2002), Stratosphere transport, *J. Meteorol. Soc. Jpn.*, *80*, 793–809.
Postel, G. A., and M. Hitchman (1999), A climatology of Rossby wave breaking along the subtropical tropopause, *J. Atmos. Sci.*, *56*(3), 359–373.
Prather, M. J. (1986), Numerical advection by conservation of second-order moments, *J. Geophys. Res.*, *91*, 6671–6681.
Prather, M., and D. Ehhalt (2001), Atmospheric chemistry and greenhouse gases, in *Climate Change 2001: The Scientific Basis*, edited by J. T. Houghton et al., pp. 239–287, Cambridge Univ. Press, New York.
Prather, M., M. McElroy, S. Wofsy, G. Russell, and D. Rind (1987), Chemistry of the global troposphere: Fluorocarbons as tracers of air motion, *J. Geophys. Res.*, *92*, 6579–6613.
Robinson, R. D. (1980), The transport of minor atmospheric constituents between troposphere and stratosphere, *Q. J. R. Meteorol. Soc.*, *106*, 227–253.
Schoeberl, M. R. (2004), Extratropical stratosphere-troposphere mass exchange, *J. Geophys. Res.*, *109*, D13303, doi:10.1029/2004JD004525.
Seo, K.-H., and K. P. Bowman (2002), Lagrangian estimate of global stratosphere-troposphere mass exchange, *J. Geophys. Res.*, *107*(D21), 4555, doi:10.1029/2002JD002441.
Sprenger, M., and H. Wernli (2003), A Northern Hemispheric climatology of cross-tropopause exchange for the ERA15 time period (1979–1993), *J. Geophys. Res.*, *108*(D12), 8521, doi:10.1029/2002JD002636.
Stohl, A., et al. (2003a), Stratosphere-troposphere exchange: A review and what we have learned from STACCATO, *J. Geophys. Res.*, *108*(D12), 8516, doi:10.1029/2002JD002490.
Stohl, A., H. Wernli, P. James, M. Bourqui, C. Forster, M. A. Liniger, P. Seibert, and M. Sprenger (2003b), A new perspective of stratosphere-troposphere exchange, *Bull. Am. Meteorol. Soc.*, *84*, 1565–1573.
Waugh, D. W., and B. M. Funatsu (2003), Intrusions into the tropical upper troposphere: Three-dimensional structure and accompanying ozone and OLR distributions, *J. Atmos. Sci.*, *60*, 637–653.
Waugh, D. W., and L. M. Polvani (2000), Climatology of intrusions into the tropical upper troposphere, *Geophys. Res. Lett.*, *27*, 3857–3860.
Wei, M.-Y. (1987), A new formation of the exchange of mass and trace constituents between the stratosphere and troposphere, *J. Atmos. Sci.*, *44*, 3079–3085.
Wild, O., J. K. Sundet, M. J. Prather, I. S. A. Isaksen, H. Akimoto, E. V. Browell, and S. J. Oltmans (2003), Chemical transport model ozone simulations for spring 2001 over the western Pacific: Comparisons with TRACE-P lidar, ozonesondes, and Total Ozone Mapping Spectrometer columns, *J. Geophys. Res.*, *108*(D21), 8826, doi:10.1029/2002JD003283.
Wild, O., et al. (2004), CTM ozone simulations for spring 2001 over the western Pacific: Regional ozone production and its global impacts, *J. Geophys. Res.*, *109*, D15S02, doi:10.1029/2003JD004041.
Wirth, V., and J. Egger (1999), Diagnosing extratropical synoptic-scale stratosphere-troposphere exchange: A case study, *Q. J. R. Meteorol. Soc.*, *125*, 635–655.
World Meteorological Organization (1985), Atmospheric ozone, *WMO Rep. 16*, Geneva, Switzerland.

J. Hsu and M. J. Prather, Earth System Science, University of California, Irvine, CA 92697, USA. (junoh@uci.edu)
O. Wild, Frontier Research Center for Global Change, JAMSTEC, Yokohama 236-0001, Japan.

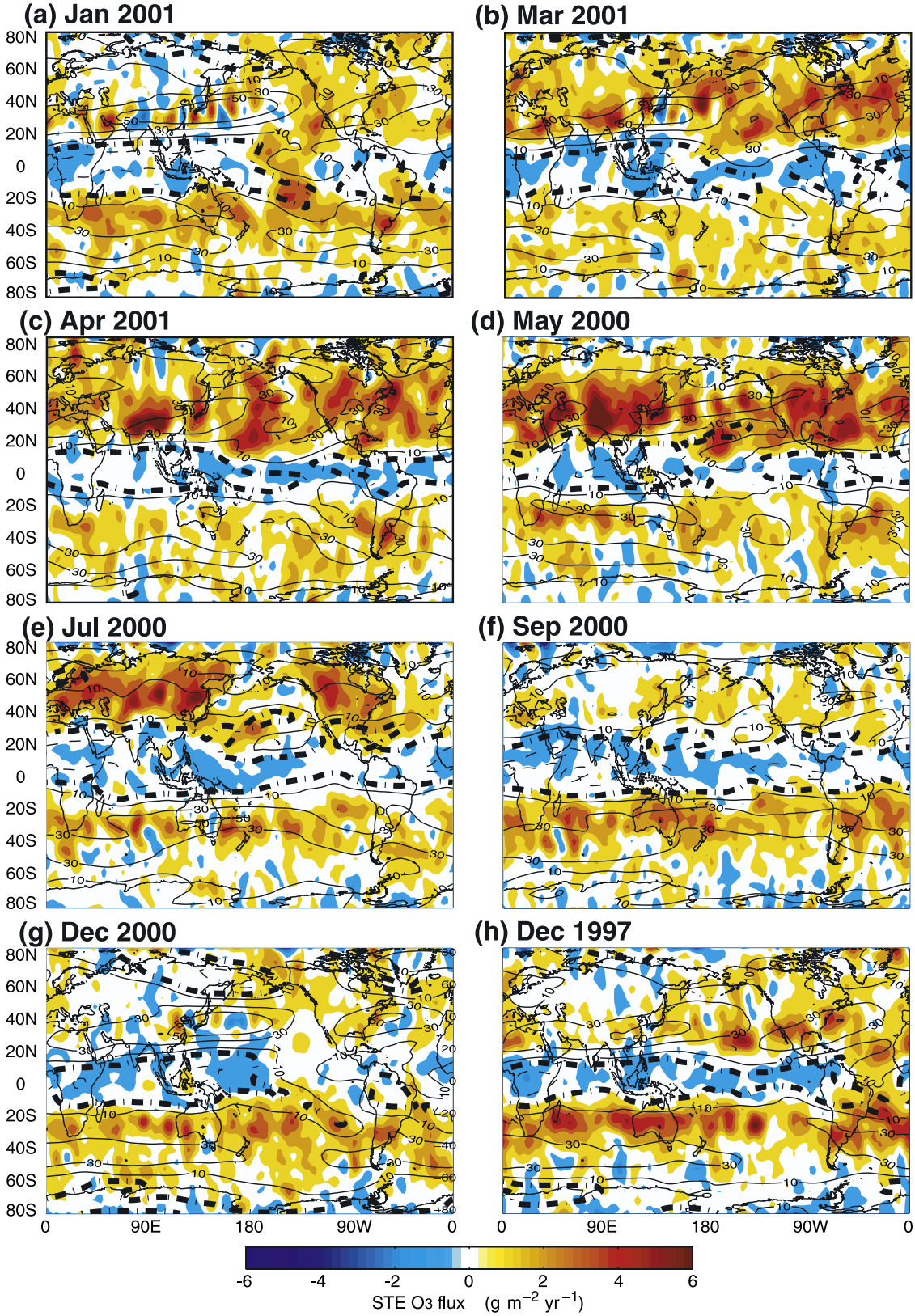

Figure 8. Color contours of monthly latitude-longitude STE flux in units of g-O_3m^{-2} y^{-1}. The color contour interval is 1. The thin solid (dashed) lines are the contours of the zonal winds (ms^{-1}) at 200 mb. The contour levels are ±10, 30, and 50. The zero wind lines are emphasized in bold dashed lines.